Control Strategies for Reactionless Capture of an Orbiting Object using a Satellite Mounted Robot

A. Gattupalli, S. V. Shah and K. M. Krishna
Robotics Research Center
International Institute of Information Technology
Hyderabad 500032, India
gattupalliaditya@gmail.com, surilshah@iiit.ac.in, mkrishna@iiit.ac.in

A. K. Misra
Mechanical Engineering Department
McGill University
Montreal, QCH3A0C3, Canada
arun.misra@mcgill.ca

***Abstract*—This paper presents a method to capture orbiting objects using a robotic system mounted on a service satellite. The main objective is to manipulate the robot such that no reaction moment gets transferred to the base satellite. This will avoid use of any attitude controller resulting in fuel savings. Note that the constraints leading to zero reaction moment are nonholonomic, and this makes path planning a complex problem. In this work, first a method based on holonomic distribution of the nonholonomic constraints is discussed. As this method exploits constraints in terms of joint velocities, it does not always ensure successful capture. Next, a method based on task-level constraints, written in terms of end-effector's velocities, has been illustrated. It is shown that the path planned using this method has several singular points. In order to overcome disadvantages of the above two methods a novel approach is proposed which uses holonomic distribution to reach closer to the target and task-level constraints to finally capture the target. Efficacy of the method is shown using a 3-link robot mounted on a service satellite.**

I. Introduction

On-orbit servicing is going to be a major operation in the coming years due to the increase in the number of satellites and space debris ([1], [2], [3]). In particular, capture and deorbiting of space debris will be an important problem in future's space missions. Collision of these debris with the operational satellites in the same orbit can cause significant damage. This calls autonomous capture of space debris using a robot mounted on service satellite before it collides with the working satellite in the same orbit. A conventional approach to control the end-effector's position is to use Generalized Jacobian Matrix(GJM) ([4], [5]) based resolved motion rate control of space manipulators .This however results in rotation of the base satellite. It is desired that there is minimum disturbance in the attitude of the base satellite during autonomous capture. This is also referred to as reactionless manipulation which results in fuel savings and increase in operating life of the satellite. In this regard, several strategies have been proposed to capture an orbiting object with minimum disturbance to the base satellite. A method of optimization was proposed in [6] for minimization of the base reactions, but it did not provide a satisfactory result on reactionless manipulation. Another attempt made in the form of disturbance map [7] lowered the fuel consumption by minimizing the attitude disturbances, and later led to a more effective extended disturbance map [8]. These maps reduce the attitude disturbance, but do not fully eliminate them. A design of manipulator was provided in [9] for reactionless manipulation where the major disadvantage was an increase in the complexity of the robot's architecture.

Another important strategy based on Reaction Null Space(RNS) to achieve reactionless manipulation was introduced in [10] and [11] for a robot with a flexible base. Later, in [12] the RNS based approach was used for the control of space robots. In [13], it was shown that zero attitude disturbance to the base satellite can be achieved using joint velocities obtained from RNS. An experimental validation of RNS based method with ETS-VII space robot and its extension to a kinematically redundant arm were presented in [13]. It was also shown that by augmenting the joint-level constraints with task-level, the end-effector can be constrained to move in a reactionless manner in the task space. However, this method can lead to several singular points, different from the dynamic singularity [14], within the robot's workspace. Optimal control for capturing objects is also proposed in [15], [16] but this may not be very helpful in real time scenarios.

It is worth noting here that the set of constraints which govern the reactionless manipulation are nonholonomic in nature and thus it is not possible to integrate them to get a set of position-level constraints. A Lie algebraic formulation of nonholonomic motion planning was presented in [17], [18]. It was shown that even though the entire set of constraints are nonholonomic, one can obtain a subset of holonomic constraints by restricting motion in some directions. This will be referred to as holonomic distribution hereafter. In this regard, a Holonomic Distribution Control (HDC) was proposed in [19] where the robot's joint space was decomposed into subsets/primitives with degree of redundancy equal to one. However, their study was limited mainly to kinematic simulations. Another limitation of their method was that the path traversed depends upon the initial conditions and may not always lead to the final position. To overcome these shortcomings, we propose a method which uses combined holonomic distribution and task-space control to achieve improved reactionless manipulation. This forms the main contribution of this work. Results of dynamic simulations are shown using the proposed approach which depicts improvement over the method used in [19].

The rest of the paper is organized as follows: Equations of motion and constraints for reactionless manipulation are provided in Section II. Reactionless capture of an orbiting object with a robotic system using holonomic distribution and task-space control and their disadvantages are presented in Section III, while the proposed method for reactionless capture

is presented in Section IV. Finally, conclusions are given in Section V.

II. Equations of Motion and constraints

In this section the dynamic equations of motion for a robot mounted on a service satellite is presented. The constraints for reactionless manipulation in terms of joint velocities (joint-level constraints) are also given and are later extended to the constraints in terms of end-effector's velocities (task-level constraints).

A. Equations of motion

The equations of motion for an n-Degrees-Of-Freedom (n-DOF) robot mounted on a floating-base is written as [13]

$$\begin{bmatrix} \boldsymbol{H}_b & \boldsymbol{H}_{bm} \\ \boldsymbol{H}_{bm}^T & \boldsymbol{H}_m \end{bmatrix} \begin{bmatrix} \ddot{\boldsymbol{x}}_{\boldsymbol{b}} \\ \ddot{\boldsymbol{\phi}} \end{bmatrix} + \begin{bmatrix} \boldsymbol{c}_b \\ \boldsymbol{c}_m \end{bmatrix} = \begin{bmatrix} \boldsymbol{F}_b \\ \boldsymbol{\tau} \end{bmatrix} + \begin{bmatrix} \boldsymbol{J}_b^T \\ \boldsymbol{J}_m^T \end{bmatrix} \boldsymbol{F}_h \tag{1}$$

where $\boldsymbol{H}_b \in R^{6\times 6}$ and $\boldsymbol{H}_m \in R^{n\times n}$ are the inertia matrices of the base and manipulator, $\boldsymbol{H}_{bm} \in R^{6\times n}$ is the coupling inertia matrix, $\ddot{\boldsymbol{x}}_b \in R^6$ is the vector of linear and angular accelerations of the base, $\ddot{\boldsymbol{\phi}} \in R^n$ is the vector of joint accelerations, $\boldsymbol{c}_b \in R^6$ and $\boldsymbol{c}_m \in R^n$ are the velocity dependent nonlinear terms of the base and manipulator, $\boldsymbol{F}_b$ and $\boldsymbol{F}_h \in R^6$ are the vectors of force and moment exerted on the centroid of the base and end-effector, $\boldsymbol{\tau} \in R^n$ is the manipulator joint torque, $\boldsymbol{J}_b \in R^{6\times 6}$and $\boldsymbol{J}_m \in R^{6\times n}$ are the Jacobian matrices for the base and manipulator.

B. Constraints for reactionless manipulation

The inertia matrix of the base and the coupling inertia matrices can also be decomposed [20] as follows:

$$\boldsymbol{H}_b = \begin{bmatrix} w\boldsymbol{E} & w\hat{\boldsymbol{r}}_{0g}^T \\ w\hat{\boldsymbol{r}}_{0g} & \boldsymbol{H}_\omega \end{bmatrix}; \quad \boldsymbol{H}_{bm} = \begin{bmatrix} \boldsymbol{J}_T \\ \boldsymbol{H}_{\omega m} \end{bmatrix} \tag{2}$$

Next, the constraints for the reactionless manipulation are derived from the conservation of the angular momentum as [13]:

$$\tilde{\boldsymbol{H}}_{bm}\dot{\boldsymbol{\phi}} = \boldsymbol{0} \tag{3}$$

where $\tilde{\boldsymbol{H}}_{bm}$ = $\boldsymbol{H}_{\omega m}$-$\hat{\boldsymbol{r}}_{0g}\boldsymbol{J}_T$. Note that (3) only ensures zero attitude disturbance, the satellite is free to move along cartesian axes. Henceforth, the reactionless manipulation will imply motion with zero attitude distribution. These constraints are converted into task-level constraints, i.e., in the space of end-effector, using a Generalised Jacobian Matrix (GJM) [5] as follows.

$$\dot{\boldsymbol{x}}_h = \boldsymbol{J}_g\dot{\boldsymbol{\phi}} \tag{4}$$

where $\boldsymbol{J}_g$ is the GJM and $\dot{\boldsymbol{x}}_h$ is the velocity of the end-effector. The GJM can be interpreted similar to the robot Jacobian for a fixed-base manipulator system, however, here the GJM contains several terms associated with the system's dynamics. Therefore by incorporating (4) into (3) we get the task-level constraints as

$$\tilde{\boldsymbol{H}}_{bh}\dot{\boldsymbol{x}}_h = \boldsymbol{0} \tag{5}$$

where $\tilde{\boldsymbol{H}}_{bh}$ = $\tilde{\boldsymbol{H}}_{bm}\boldsymbol{J}_g^{-1}$ and the GJM is assumed to be invertible or pseudo inverse can be used otherwise.

III. Reactionless Capture of an Orbiting object

In this section, three approaches for reactionless capture of an orbiting object and their shortcomings are discussed in detail.

A. Joint-space control

Solution of (3) provides joint motions which lead to reactionless manipulation. The number of joints that can be independently controlled is determined by the Degree-of-Redundancy (DOR) associated with (3). In the case of planar 3-link robot mounted on a satellite, DOR is 2. This is due to the fact that only one component of the base angular velocity is constrained. Therefore any two joints can be controlled independently. One way of solving (3) is to partition it in terms of independent ($\dot{\boldsymbol{\phi}}^i$) and dependent ($\dot{\boldsymbol{\phi}}^d$) joint rates as

$$\begin{bmatrix} \tilde{\boldsymbol{H}}_{bm}^d & \tilde{\boldsymbol{H}}_{bm}^i \end{bmatrix} \begin{bmatrix} \dot{\boldsymbol{\phi}}^d \\ \dot{\boldsymbol{\phi}}^i \end{bmatrix} = \boldsymbol{0} \tag{6}$$

Now, given the independent joint rates , the dependent joint rates can be obtained as

$$\dot{\boldsymbol{\phi}}^d = -\tilde{\boldsymbol{H}}_{bm}^{d^{-1}}\tilde{\boldsymbol{H}}_{bm}^i\dot{\boldsymbol{\phi}}^i \tag{7}$$

Alternatively one may also use pseudo inverse [13]. It is worth noting that joint-space control using co-ordinate partitioning or pseudo inverse cannot lead to a trivial solution for desired motion of the end-effector from initial to final position. Another approach is to use Holonomic Distribution Control (HDC) as proposed in [19]. The HDC is described in the following subsection.

B. Holonomic distribution control

For the nonholonomic system represented by (3), space of allowable motion is given by the directions in which it can move freely. This space is the right null space denoted as $\boldsymbol{g}_j(\boldsymbol{\phi})$ of the reactionless constraints in (3), i.e.,

$$\tilde{\boldsymbol{H}}_{bm_i}(\boldsymbol{\phi})\boldsymbol{g}_j(\boldsymbol{\phi}) = \boldsymbol{0} \tag{8}$$

where $i = 1, 2, ..., m$ and $j = 1, 2, 3...., n-m$. Hence the allowable space is given by

$$\dot{\boldsymbol{\phi}} = \boldsymbol{g}_1(\boldsymbol{\phi})\boldsymbol{u}_1 + \boldsymbol{g}_2(\boldsymbol{\phi})\boldsymbol{u}_2 + ... + \boldsymbol{g}_r(\boldsymbol{\phi})\boldsymbol{u}_r \tag{9}$$

Here $r = n - m$ is the DOR, n is the DOF of the robot and m is the number of task constraints. Here $\boldsymbol{g}_i$ are the vector fields forming the range space of $\boldsymbol{g}$. A vector field on R^n is a smooth map which assigns a map from ϕ to tangent vector $\dot{\phi} \in T_\phi R^n$ [21] where $T_\phi R^n$ stands for tangent space. A distribution is defined as a map from linear sub space of $T_\phi R^n$ to the configuration space ϕ [21]. An example of a distribution is

$$\triangle = Span[\boldsymbol{g}_1, \boldsymbol{g}_2.....\boldsymbol{g}_r] \tag{10}$$

The distribution $\triangle_{\boldsymbol{\phi}}$ is the subspace of $\triangle$ evaluated at configuration $\boldsymbol{\phi}$ where $\triangle_{\boldsymbol{\phi}} \subset T_\phi R^n$. A distribution is regular if the dimension of $\triangle_{\boldsymbol{\phi}}$ does not vary with $\boldsymbol{\phi}$ and is involute if it is closed under Lie Bracket which is defined as follows:

$$[\boldsymbol{g}_1, \boldsymbol{g}_2] = \frac{\partial \boldsymbol{g}_1}{\partial \boldsymbol{\phi}}\boldsymbol{g}_2 + \frac{\partial \boldsymbol{g}_2}{\partial \boldsymbol{\phi}}\boldsymbol{g}_1 \tag{11}$$

Frobenious theorem states that the distribution $\triangle$ is integrable if and only if it is involute. The concept of holonomic distribution is based on achieving subset of integrable constraints from a set of nonholonimic constraints by restricting motion in some directions. The dimension of the distribution $\triangle$ is defined using the DOR, r. One dimensional distributions are used because the reactionless motion evolves from a one dimensional manifold or a simple curve. Using the column vectors of $\tilde{\boldsymbol{H}}_{bm}$ the involutivity of the one dimensional distribution $\triangle_1$ was established in [11]. Therefore, $\triangle_1$ is integrable from the Frobenius theorem. Here, our objective is to find one dimensional distributions $\triangle_1$ so that the motion can be steered in different directions and is also unique. The concept of primitives to define these one dimensional distributions was proposed in [19]. A primitive consists of m+1 joints which are actuated at a given time while the other joints are servo locked. So for a 3-DOF planar robot there are 3 primitives defined which are P_1 (joints 1 and 2 are actuated), P_2 (joints 1 and 3 are actuated) and P_3 (joints 2 and 3 are actuated), respectively. For a higher dimensional distributions, the reactionless paths lie in higher dimensional manifolds. To choose an appropriate direction in these higher dimensional manifolds is a difficult problem which is avoided. Equation (3) can be rewritten in terms of the stationary and the actuated joints as

$$\begin{bmatrix} \tilde{\boldsymbol{H}}^{s}_{bm} & \tilde{\boldsymbol{H}}^{a}_{bm} \end{bmatrix} \begin{bmatrix} \dot{\boldsymbol{\phi}}^{s} \\ \dot{\boldsymbol{\phi}}^{a} \end{bmatrix} = \boldsymbol{0} \tag{12}$$

For stationary joints $\dot{\boldsymbol{\phi}}^{s}$ is zero and

$$\dot{\boldsymbol{\phi}}^{a} = (\boldsymbol{E} - \tilde{\boldsymbol{H}}^{a+}_{bm}\tilde{\boldsymbol{H}}^{a}_{bm})\dot{\boldsymbol{\zeta}} \tag{13}$$

where $(\boldsymbol{E} - \tilde{\boldsymbol{H}}^{a+}_{bm}\tilde{\boldsymbol{H}}^{a}_{bm})$ is the null space projector and $\dot{\boldsymbol{\zeta}} \in R^{m+1}$ is an arbitrary column vector. For the controlled dynamics simulation, the trajectory following proportional and derivative control law is used as

$$\boldsymbol{\tau}_i = K_p(\boldsymbol{\phi}_d - \boldsymbol{\phi}) + K_d(\dot{\boldsymbol{\phi}}_d - \dot{\boldsymbol{\phi}}) \tag{14}$$

Here $\boldsymbol{\phi}_d$ and $\dot{\boldsymbol{\phi}}_d$ are the desired joint angles and joint rates obtained from (13) whereas $\boldsymbol{\phi}$ and $\dot{\boldsymbol{\phi}}$ are the actual values of joint angles and joint rates obtained from the dynamic simulation. K_p and K_d are proportional and derivative gains and are taken empirically as 49 and 14, respectively.

The path planning algorithm is devised such that the end-effector reaches a desired point using a set of primitives. For path planning of the 3-DOF planar robot mounted on the satellite, six different primitives are chosen as $P_{\pm1}, P_{\pm2}, P_{\pm3}$ where the sign denotes whether the end-effector is moving in the clockwise or anti clockwise direction as indicated in Fig. 1. In contrast to [19], here the algorithm iteratively chooses the primitive which generates the closest point to the desired target point. The algorithm is illustrated in Algorithm 1.

A dynamic simulation is carried out using the following initial joint angles as $\boldsymbol{\phi}_{initial}$=$[-1.3, 2.9, 2.6]rad$ and the final end-effector position as $\boldsymbol{x}_{desired}$=$[2.8, -0.5]m$. The mass of the satellite is 500 Kg while the mass of each link is taken as 10 Kg. The time step $\triangle t$ is taken to be 5 seconds. The path traced by end effector is shown in Fig. 2. The joint angles and joint rates of the arm are provided in Fig. 3 whereas the joint

Step 1 $\rightarrow$ Initialize t_0 = 0 and appropriate initial conditions x_{b_i} and ϕ_i.
Step 2 $\rightarrow$ Using current state variables at time t_i which are $\boldsymbol{x}_b$, $\boldsymbol{\phi}$ calculate the inertia matrices $\boldsymbol{H_b}$, $\boldsymbol{H}_{bm}$ and $\boldsymbol{H}_m$ along with the constraint matrix $\tilde{\boldsymbol{H}}_{bm}$.
Step 3 $\rightarrow$ Using the input $\dot{\boldsymbol{\zeta}}$ calculate the values of $\dot{\boldsymbol{\phi}}_p$ for each of the six primitives $P_{\pm i}$ where $i = 1, 2, 3$.
Step 4 $\rightarrow$ Using different primitive values using the torques in (14) system is dynamically evolved for $t = \triangle t$ using ReDySim [22] simulation package.
Step 5 $\rightarrow$ Calculate the time and the corresponding distance for each of the primitives where distance between the end-effector and the goal point is the least. Among the six primitives choose the primitive P_i which gives minimum distance to the goal.
Step 6 $\rightarrow$ Stop, if the end-effector reaches the goal. Otherwise, go to Step 2 taking $t = t_i$, $\boldsymbol{x}_{bi}$ and $\boldsymbol{\phi}_i$ from the primitive P_i

Algorithm 1: Path planning using holonomic distribution

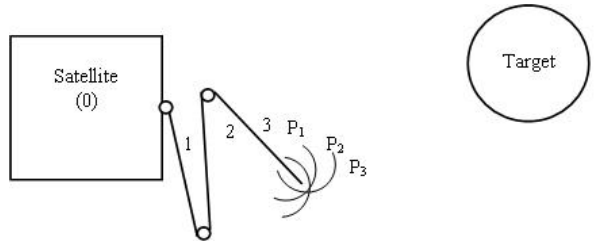

Fig. 1: Different path primitives for a 3-DOF planar robot

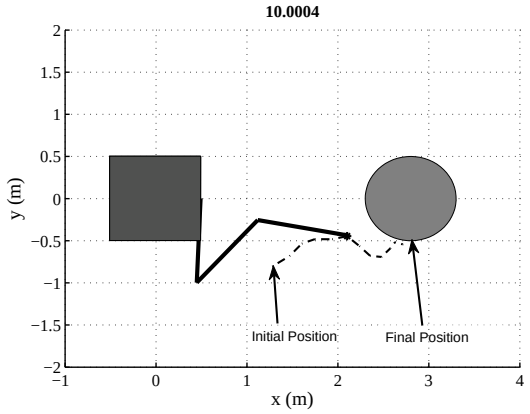

Fig. 2: End-effector's path using holonomic distribution control

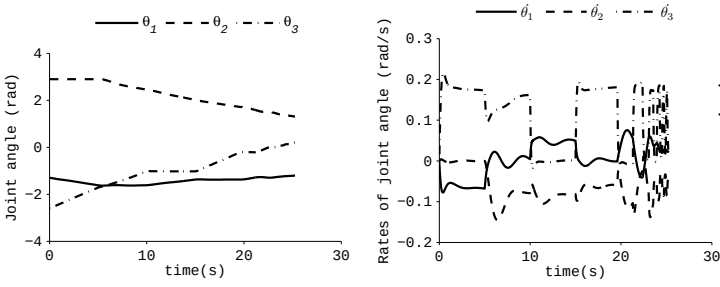

(a) Joint Angles (b) Joint Rates

Fig. 3: Joint motions using holonomic distribution control

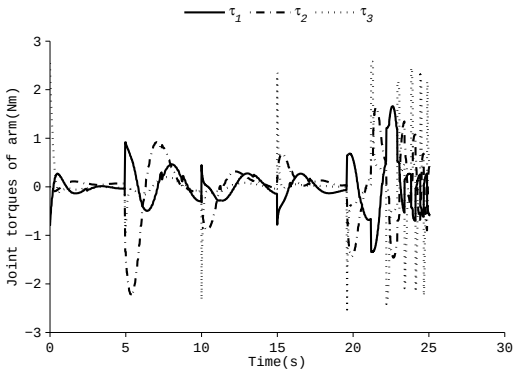

Fig. 4: Joint torques using holonomic distribution control

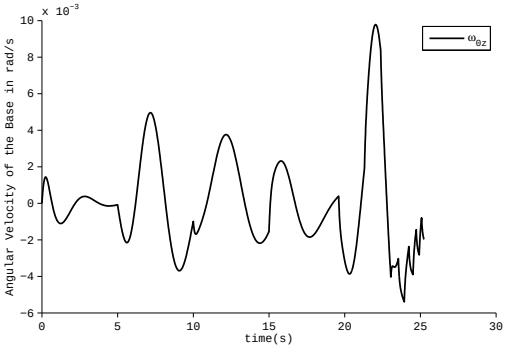

Fig. 5: Base angular velocity using holonomic distribution control

torques corresponding to these joint rates are given in Fig. 4 which are derived according to the PD control law in (14)

It is worth noting that when the end-effector approaches closer to the target point, the frequency of switching between primitives increases. This results into sudden change in the joint velocities as shown in Fig. 3b and lead to non-smooth joint torques as shown in Fig. 4. This can disturb the attitude of the base satellite when the end-effector is about to intercept the target point. This is also evident from Fig. 5. Moreover, path planning using joint-primitives can not always lead to the final position. This is another limitation of this method.

C. Task-space control

In this section, the reactionless manipulation using task-level constraints of (5) is presented. To achieve task-level reactionless manipulation we use co-ordinate partitioning where the end-effector velocity space is partitioned into independent and the depended velocity components as

$$\begin{bmatrix} \tilde{\boldsymbol{H}}^{d}_{bh} & \tilde{\boldsymbol{H}}^{i}_{bh} \end{bmatrix} \begin{bmatrix} \dot{\boldsymbol{x}}^{d}_{h} \\ \dot{\boldsymbol{x}}^{i}_{h} \end{bmatrix} = 0 \tag{15}$$

Next, the dependent velocities are obtained in terms of independent velocities as

$$\dot{\boldsymbol{x}}^{d}_{h} = -\tilde{\boldsymbol{H}}^{d^{-1}}_{bh} \tilde{\boldsymbol{H}}^{i}_{bh} \dot{\boldsymbol{x}}^{i}_{h} \tag{16}$$

In the case of planar 3-DOF space robot the independent velocities ($\dot{\boldsymbol{x}}^{i}_{h}$) of the end-effector are taken as $\boldsymbol{v}_x, \boldsymbol{v}_y$ whereas the dependent velocity ($\dot{\boldsymbol{x}}^{d}_{h}$) is taken as ω. The value of $\dot{\boldsymbol{x}}^{i}_{h}$ is defined using an interpolating polynomial as

$$\dot{\boldsymbol{x}}(t) = a + 3b\Big(\frac{t}{T}\Big)^2 + 4c\Big(\frac{t}{T}\Big)^3 + 5d\Big(\frac{t}{T}\Big)^4 \tag{17}$$

where $a = \dot{\boldsymbol{x}}_I, b = 10v - (6\dot{\boldsymbol{x}}_I + 4\dot{\boldsymbol{x}}_F), c = -15v + (8\dot{\boldsymbol{x}}_I + 7\dot{\boldsymbol{x}}_F), d = 6v - (3\dot{\boldsymbol{x}}_I + 3\dot{\boldsymbol{x}}_F)$ and $v = \frac{[\boldsymbol{x}_F - \boldsymbol{x}_I]}{T}$. ($\boldsymbol{x}_I$ and $\boldsymbol{x}_F$) and ($\dot{\boldsymbol{x}}_I$ and $\dot{\boldsymbol{x}}_F$) are the initial and final positions and velocities, respectively. Given the initial and final configurations of the independent end-effector velocities one can find the dependent velocities using (16). Simulation was performed for the same initial joint angles and the final end-effector position taken in the previous subsection. The initial and final velocities are assumed to be zero and simulation time is taken t=30s. The joint angles and joint rates are given in Fig. 6 while the joint torques required are shown in Fig. 7.

Here, the simulation failed to proceed beyond 25 s and joint torque approached to infinity, as evident form Fig. 7. In order to get further insight, the singularity index of the coefficient matrix is calculated as

$$S = \sqrt{det(\tilde{\boldsymbol{H}}^{d}_{bh} \tilde{\boldsymbol{H}}^{d^T}_{bh})} \tag{18}$$

The singularity index is plotted in Fig. 8, which shows that the index becomes zero after 25 s. This corresponds singular configuration and is due to the non invertibility of the coefficient matrix $\tilde{\boldsymbol{H}}^{d}_{bh}$ (16). Note that (16) is highly constrained and the path obtained using it can have several singular points as illustrated above. Therefore task-level planning cannot always lead to a nonsingular path. Next, an alternative approach is presented which helps in overcoming the disadvantages associated with holonomic distribution and task-space control.

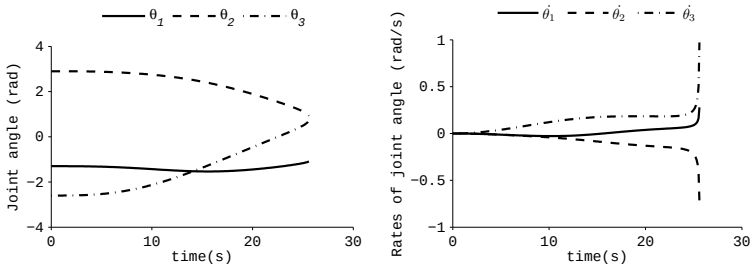

(a) Joint Angles (b) Joint Rates

Fig. 6: Joint motions using task-space control

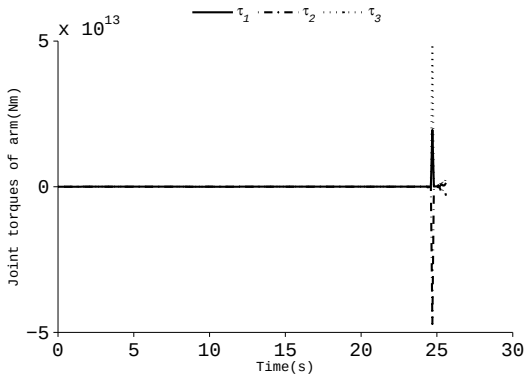

Fig. 7: Joint torques using task-space control

IV. HYBRID HOLONOMIC DISTRIBUTION AND TASK-SPACE CONTROL

In this method, path planning is done in two stages. In the first stage, the end-effector travels closer to the target point using joint primitives, while in the second stage, the path is planned using the task-level constraints. This not only ensures smooth transition but also is able to avoid singular configuration. Hence, the proposed method overcomes disadvantages of both holonomic distribution and task-space control. The method is illustrated next using the problem solved in the previous section.

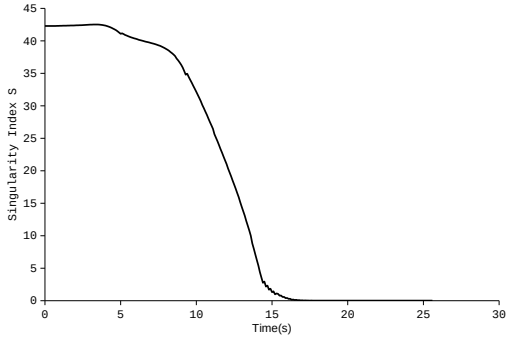

Fig. 8: Singularity Index

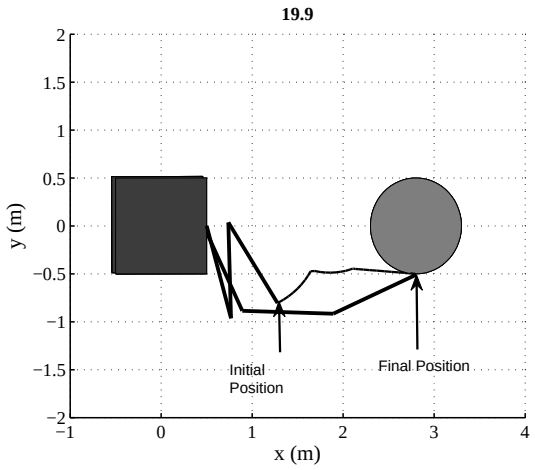

Fig. 9: End-effector's path using hybrid control

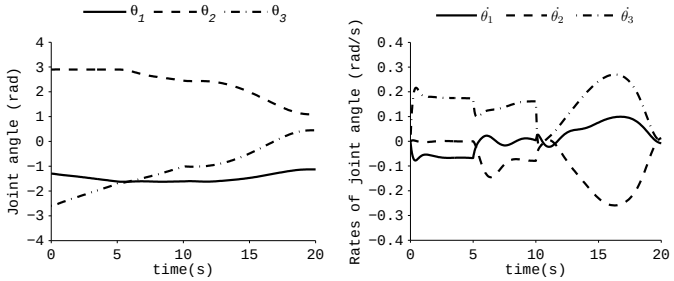

(a) Joint Angles (b) Joint Rates

Fig. 10: Joint motions using hybrid control

A dynamic simulation is carried out using the initial joint angles as $\boldsymbol{\phi}_{initial}$=$[-1.3, 2.9, 2.6]rad$ and the final end-effector position as $\boldsymbol{x}_{desired}$=$[2.8, -0.5]m$. For the first $10s$ the method of joint-primitives is used to move the end-effector closer to the target point and after that for another $10s$ the task-level constraints are used. The path traversed by the end-effector is shown in Fig. 9. The joint rates and joint angles corresponding to this path can be seen in Fig. 10 which shows that the transition in the joint velocities is much smoother than what is obtained in Fig. 3. This is also evident from the results for joint torques in Fig. 11. Here, the joint torques are continuous as compared to the same obtained using only HDC in Fig. 4. This resulted into improved reactionless manipulation as the maximum change in the base angular velocity, as shown in Fig. 12, is half of the same obtained using HDC. The singularity index is also plotted in Fig. 13 which shows that the robot stays away from singular configuration throughout the simulation period. This proves the efficacy of the proposed method.

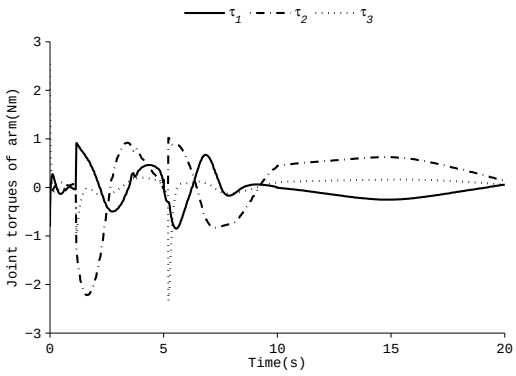

Fig. 11: Joint torques using hybrid control

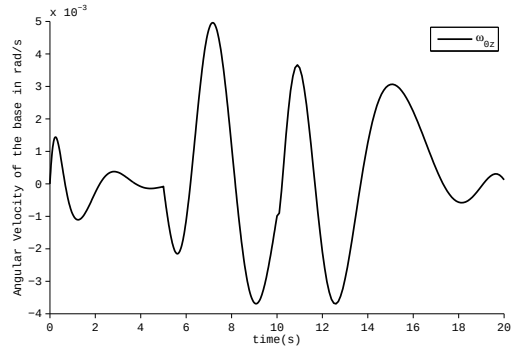

Fig. 12: Base angular velocity using hybrid control

V. Conclusion

A novel method has been proposed in this work to capture an orbiting object in a reactionless manner. The method utilizes holonomic distribution to move close to the target, and task-space control to capture the object. It is shown that the proposed approach is better than both holonomic distribution which has high discontinuities in joint velocities, and task-space control which suffers from singularities. The method is illustrated using a 3-link robot mounted on a satellite. It has been shown that the joint torques required in the proposed method are smooth in comparison to holonomic distribution. This resulted in improved reactionless manipulation as evident from the plot of angular velocity of the base satellite. The method will be implemented for reactionless manipulation of a 7-DOF redundant robotic arm in future work. Experimental implementation of the proposed method for control of an earth-based 3-link robot will also be carried out in future.

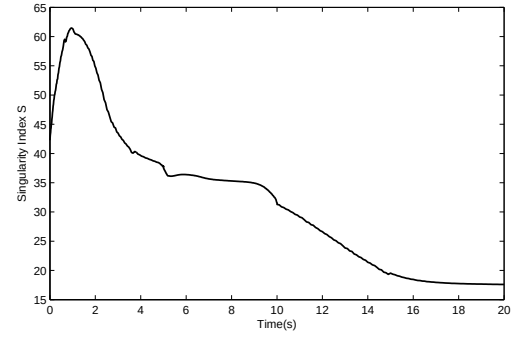

Fig. 13: Singularity Index

References

[1] F. Sellmaier, T. Boge, J. Spurmann, S. Gully, T. Rupp and F. Huber, "On-Orbit Servicing Missions: Challenges and Solutions for Spacecraft Operations," AIAA SpaceOps Conference, pp. 25-30, 2010.

[2] "On-Orbit Satellite Servicing Study," NASA Project Report, 2010.

[3] J. Liou, "An Active Debris Removal Parametric Study for LEO Environment Remediation," Advances in Space Research, 47(11), pp. 1865-1876, 2011.

[4] S. K. Saha, "A Unified Approach to Space Robot Kinematics," Transactions on Robotics and Automation, 12(3),401-405, 1996.

[5] Y. Umetani and K. Yoshida, "Resolved Motion Rate Control of Space Manipulators with Generalized Jacobian Matrix," IEEE Transactions on Robotics and Automation, 5(3), pp. 303-314, 1989.

[6] C. L. Chung, S. Desa, and C. W. deSilva, "Base Reaction Optimization of Redundant Manipulators for Space Applications," The Robotic Institute CMU-RI-TR, pp. 88-17, 1988.

[7] S. Dubowsky, and M. A. Torres, "Path Planning for Space Manipulators to Minimize Spacecraft Attitude Disturbances," IEEE International Conference on Robotics and Automation, pp. 2522-2528, 1991.

[8] M. A. Torres and S. Dubowsky, "Minimizing Spacecraft Attitude Disturbances in Space Manipulator Systems," Journal of Guidance, Control, and Dynamics, 15(4), pp. 1010-1017, 1992.

[9] E. Papadopoulos, and A. Abu-Abed, "Design and Motion Planning for a Zero-reaction Manipulator," IEEE International Conference on Robotics and Automation, pp. 1554-1559, 1994.

[10] D. N. Nenchev, K. Yoshida, and M. Uchiyama, "Reaction Null-space based Control of Flexible Structure Mounted Manipulating Systems," IEEE CDC, pp. 4118-4123, 1996.

[11] D. N. Nenchev, and K. Yoshida, "Reaction Null-space Control of Flexible Structure Mounted Manipulator Systems," IEEE Trans. on Robot. and Automat., 15(6), pp. 1011-1023, 1999.

[12] D. N. Nenchev and K. Yoshida, "Impact Analysis and Post-impact Motion Control Issues of a Free-floating Space Robot Subject to a Force Impulse," IEEE Transactions on Robotics and Automation, 15(3), pp. 548-557, 1999.

[13] K. Yoshida, K. Hashizume and S. Abiko, "Zero Reaction Maneuver: Flight Validation with ETS-VII Space Robot and Extension to Kinematically Redundant Arm," IEEE International Conference on Robotics and Automation, pp. 441-446, 2001.

[14] E. Papadopoulos and S. Dubowsky, "Dynamic Singularities in Free-floating Space Manipulators," Journal of Dynamic Systems, Measurement and Control, 115(1), pp. 44-52, 1993.

[15] P. Huang, J. Yan, J. Yuan and Y. Xu, "Robust Control of Space Robot for Capturing Objects Using Optimal Control Method," IEEE International Conference on Information Acquisition, pp. 397-402, 2007.

[16] P. Huang; K. Chen; Y. Xu, "Optimal Path Planning for Minimizing Disturbance of Space Robot," 9th International Conference on Control, Automation, Robotics and Vision, pp. 1-6, 2006.

[17] Y. Nakamura, R. Mukherjee, "Nonholonomic Path Planning of Space Robots via a Bidirectional Approach," IEEE Transactions on Robotics and Automation, 7(4), pp. 500-514, 1991.

[18] R. W. Murray, and S. S. Sastry, "Nonholonomic Motion Planning: Steering Using Sinusoids," IEEE Transactions on Automatic Control, 38(5), pp. 700 - 716, 1993.

[19] D. Dimitrov and K. Yoshida, "Utilisation of Holonomic Distribution Control for Reactionless Path Planning," IEEE International Conference on Intelligent Robots and Systems, pp. 3387-3392, 2006.

[20] D. Dimitrov and K. Yoshida, " Momentum Distribution in a Space Manipulator for Facilitating the Post-Impact Control," IEEE International Conference on Intelligent Robots and Systems, pp. 3345-3350, 2004.

[21] R. W. Murray, Z. Li, and S. S. Sastry "A Mathematical Introduction to Robotic Manipulation," CRC Press, Boca Raton, FL, 1993.

[22] S. V. Shah, P. V. Nandhial and S. K. Saha, "Recursive Dynamics Simulator (ReDySim)-A Multibody Dynamics Solver," Theoretical and Applied Mechanics Letters, 2(6), pp. 063011(1-6), 2012.